Geophysical Research Letters

Supporting Information for

Induced seismicity associated with hydraulic fracturing for shale gas in northwest England: an alternative view

Rob Westaway

School of Engineering, University of Glasgow, James Watt (South) Building, Glasgow G12 8QQ, U.K.

e-mail: robert.westaway@glasgow.ac.uk

Contents of this file

Introduction

Supplementary text S1 explains in detail the procedures that I have used for determining hypocentral locations and focal mechanism orientations, for induced microerthquakes that occurred near the Preese Hall-1 borehole in 2011.

Figure S1 depicts a number of alternative projections of the focal mechanism determined by *Seismik* [2012] and *Clarke et al*. [2014] for the 2 August 2011 event. It is provided as an aid to understanding regarding possible resolutions of the issue of what orientation this focal mechanism is actually supposed to have.

Figure S2 depicts a candidate solution for the focal mechanism of the 2 August 2011 event, which was considered but is not preferred, for reasons set out in detail in supplementary text S1.

Figure S3 depicts the focal mechanism of the 27 May 2011 event, as determined by *O'Toole et al*. [2013]. It is provided here to facilitate discussion in supplementary text S1, as the original authors did not illustrate the orientation of the S-wave radiation patterns.

Table S1 lists the co-ordinates of the temporary seismograph stations that operated during 2011 in the vicinity of the Preese Hall-1 borehole.

Table S2 lists arrival time picks, modeled source parameters, and modeled ray path geometries to the seismograph stations listed in Table S1, for seismic phases radiated by the 2 August 2011 event, given the velocity model depicted in Table 1 in the main text.

Text S1

Arguably the most significant issues affecting the *Clarke et al*. [2014] paper concern the procedures used to determine the hypocenter and focal mechanism of the induced seismicity. As well as the 2 August 2011 event, *Clarke et al*. [2014] discussed some of the other induced earthquakes that were large enough to be recorded by the regional seismograph network operated by the British Geological Survey (BGS). However, as *Clarke et al*. [2014] did not provide absolute timing for the seismograms that they displayed, it is impossible to compare their identifications of seismic phases with those provided independently by BGS [*Galloway*, 2012]. Some of these induced earthquakes were also recorded by a temporary seismograph network (see the present Table S1 or Fig. 1 of *Clarke et al*. [2014]) comprising four stations: PRH some ~250 m west of the Preese Hall-1 wellhead; HHF some ~1000 m to the south; AVH some ~1300 m to the NNW; and EVW some ~2800 m to the east.

The first report on this induced seismicity, by *Eisner et al*. [2011], placed the activity beneath the area between PRH and HHF, centered maybe ~400 m south of the wellhead, their locations being obtained using a conventional layered velocity model. The subsequent *Seismik* [2012] report proposed on no clear basis that the local velocity structure is strongly anisotropic, with azimuthal variations in seismic velocities of ~20%, a factor not considered by *Eisner et al*. [2011]. On this basis they determined a new location, ~500 m east of the wellhead and ~300 m east of the bottom of the well, the basal part of which inclines eastward. The *Clarke et al*. [2014] epicenter is different yet again; it is ~600 m east of the wellhead (i.e., near the *Seismik* [2012] location), although there is no suggestion in their analysis that the seismic velocity structure is anisotropic. A further difficulty concerns the focal depth, which *Clarke et al*. [2014] determined as ~2930 m. This placed the earthquake that they analysed more than 150 m below the well bottom (at 2773 m depth), almost 200 m below the base of the Bowland Shale (at 2744 m depth, according to the borehole log; Table 1), the rock unit being fracked, and even farther below the depths at which fracking took place (*de Pater and Baisch* [2011] stated that the well was perforated as deep as 2728 m for the first fracking stage and as shallow as 2380 m for the fifth). It would appear that the cause of this apparent anomaly is the use by *Clarke et al*. [2014] of an inappropriate seismic velocity structure. Shallower than 2520 m depth, they used seismic velocities derived from logging of the Preese Hall-1 borehole, but at greater depths they adopted P- and S-wave velocities of 5.90 km s^{-1} and 3.49 km s^{-1}, respectively, from a BGS regional model [e.g., *Galloway*, 2012]. These parameters would be appropriate for Lower Paleozoic metamorphic basement, but have been used by *Clarke et al*. [2014] at depths that correspond to Carboniferous sediments, within which much lower velocities are appropriate. Indeed, according to *Kirby et al*. [2000], Lower Paleozoic metamorphic basement is only reached in this area at depths in excess of 5000 m.

It is well-known in earthquake seismology that use of a seismic velocity model that is 'too fast' will result in hypocenters that are too far from the recording stations. In this case, for seismicity located inside the recording network, the systematic error that can be anticipated is for the true focal depth to be overestimated by the location procedure. The procedure used by *Clarke et al.* [2014] contrasts with that adopted by *Eisner et al*. [2011], who defined a velocity model in which P- and S-wave velocities appropriate for the Bowland Shale were assumed to persist to a depth of 7500 m, well below the greatest conceivable depth encountered by any seismic phase of interest, recorded by any local station. With this original velocity model, *Eisner et al*. [2011] obtained focal depths of ~2200-2400 m, more in keeping with what might be expected given that the induced fractures tend to propagate upward from the borehole perforations at which they initiate [e.g., *Fisher and Warpinski*, 2012; *Westaway and Younger*, 2014]. For comparison, *O'Toole et al*. [2013] obtained a focal depth of 2343±2 m for the 27 May 2011 event using the *Eisner et al*. [2011] velocity model. To facilitate discussion, I locate the 2 August 2011 event again, using the seismic velocity model in Table 1, the results being presented in Table S2.

As regards the location procedure for the 2 August 2011, the data presented by *Clarke et al*. [2014] (in their online supplement 2) indicate very similar P-wave arrival times at AVH, PRH and HHF and a later arrival time at EVW. However, given the geometry of the stations, unless the seismic velocity structure is strongly

anisotropic (an aspect that *Clarke et al*. [2014] did not mention), any hypocenter that is roughly equidistant from AVH and HHF will be significantly closer to PRH than to these other stations, calling this interpretation into question. Furthermore, the P-wave arrival times picked by *Clarke et al*. [2014] do not always correspond to clear seismic signals, especially at station AVH. There are clear S-wave arrivals at HHF and PRH but the arrival time picks by *Clarke et al*. [2014] again do not seem to match the actual arrival times of the seismic phases. I have re-picked the arrival times (Table S2); it is thus found that the S-wave arrival at HHF precedes that at PRH by some ~70 ms. In the absence of an appeal to evidence to the contrary (from anisotropy or some other cause of lateral variation in the velocity structure) this indicates that the hypocenter is closer to HHF than to PRH, leading to the conclusion that its location was most likely somewhere between the two stations, south or SSE of PRH and north or NNW of HHF. This is roughly where both *Eisner et al*. [2011] and *O'Toole et al*. [2013] placed the seismic activity but different from the location proposed by *Clarke et al*. [2014].

Table S2 indicates that a hypocenter circa British National Grid reference SD 3772 3584, at a depth of ~2500 m, with an origin time circa 9.36 s on the timescale used for display of the seismograms in online supplement 2 of *Clarke et al*. [2014], can achieve a reasonable fit to the data. The fit is better to the S-wave data than to the P-wave data, suggesting that the latter, which are indistinct, may have been picked incorrectly. Alternatively, the P-wave arrivals at PRH and AVH somewhat earlier than expected might indicate a faster seismic velocity structure for waves travelling upward to the north or northwest than for those travelling upward to the south or southeast. Such a variation might well be expected given the northwestward thinning of the low-velocity Bowland Shale evident from the seismic section in Fig. 4 of *Clarke et al*. [2014].

In detail, the corresponding epicenter, some 800 m south of the Preese Hall-1 wellhead, is a few hundred meters south of the locations of the earlier events in the sequence as reported by *Eisner et al*. [2011]. This pattern of locations implies that the induced fractures extended southward from the borehole, in alignment with the maximum principal stress, intersecting the fault in this vicinity; some of the fracking fluid presumably 'bled' from the induced fracture into the fault and increased the pore pressure on a patch of the fault plane, inducing the coseismic slip. Conversely, given the orientation of the local stress field (see the main text) it is difficult to see how any induced fracture could have reached any point hundreds of meters east of and hundreds of meters deeper than the borehole perforations at which the fracking fluid was injected, as is implied by the hypocentral solution reported by *Clarke et al*. [2014]. Clearly, my revised solution is non-unique, but in the absence of any three-dimensional model for the P- and S-wave velocities in the locality (which vary independently, given that different lithologies present have significantly different Poisson's ratios; Table 1), it is difficult to see what more can be done, using the available data, to locate this seismicity. The necessity for three-dimensional seismic velocity control (not to mention, for better integration between any layered velocity model and the principal stratigraphic boundaries in the area; cf. Table 1) should, however, be noted in connection with plans for microseismic monitoring of future shale gas developments in adjacent localities.

Like *Seismik* [2012] (Fig. S1(a)), *Clarke et al*. [2014] (Fig. S1(b)) based their focal mechanism on polarities and amplitudes of P-waves at AVH, PRH, and HHF and S-waves at PRH and HHF. However, it should be evident that use of amplitudes in such analysis is dependent on knowledge of the extent to which seismic waves experience anelastic attenuation along their propagation paths. No details of how attenuation was quantified were provided and the citation of a reference for the algorithm used was unhelpful as no associated reference details were provided. Furthermore, according to the discussion in their online supplement 2, although their solution correctly matched the S-wave polarities at PRH and HHF and the compressional P-wave polarity they picked at HHF, it did not match their picks of P-wave dilatation at PRH and compression at AVH. Of course, if their hypocenter was mislocated, as suggested above, the seismograph stations will not have been plotted in the correct places on the focal sphere and the focal mechanism will also be incorrect. An additional reason for calling their focal mechanism into question is that when it is plotted correctly

according to the stated angular measurements (Fig. S1(c)) the maximum principal stress falls within its compressional quadrant. A possible reason for this is that these authors have in fact drawn upper focal hemisphere projections even though these are labelled as lower focal hemisphere projections but, if so, they must also have defined rake using a left-handed sign convention, rather than the right-handed standard used in earthquake seismology (Fig. S1(c)-(e)); if so, then their actual focal mechanism has strike 040°, dip 70° and rake -30°.

The P-wave first motions from the 2 August 2011 event are not straightforward to pick as it is difficult to decide which pulse of radiated seismic energy is the first to exceed the background noise. The clearest depiction of these data is that by *Seismik* [2012]; these authors reported compressional first motions at AVH and HHF and dilatation at PRH, interpretations that were supported by *Clarke et al*. [2014]. On the other hand, the arrival time picks illustrated by *Seismik* [2012] seem to be preceded by earlier seismic signals, suggesting that they have been picked too late. In my view, based on these illustrations of the seismograms, the earliest P-wave pulses appear to be low amplitude dilatations at AVH, HHF and EVW and a stronger compression at PRH. I thus suggest, for example, that the true P-wave first motion at HHF is the dilatational pulse visible in Fig. B1 of online supplement 2 of *Clarke et al*. [2014] some 25 ms earlier than their arrival time pick. This is, indeed, the first pulse large enough to exceed the background noise level; furthermore, an earlier P-wave arrival time at HHF would eliminate the discrepancy evident in the *Clarke et al*. [2014] interpretation, whereby the S-wave arrival is earlier at HHF than at PRH but the P-wave arrivals were picked later at HHF than at PRH.

The S-waves at HHF show clear pulses to the east on the east component and to the north on the north component (see Fig. B1 in online supplement 2 of *Clarke et al*. [2014]), which both *Seismik* [2012] and *Clarke et al*. [2014] took as the first motions. Given the standard definition of S-wave polarities [*Aki and Richards*, 1980, p. 114] and the up-to-the-south propagation to this station, negative SH-polarity and positive SV-polarity are thus indicated. On the other hand, the same seismograms show these pulses to be preceded by much lower amplitude pulses of opposite polarity; if *these* are the true first motions then this station indicates positive SH-polarity and negative SV-polarity. Furthermore, at PRH the initial S-wave signal appears as a southward pulse on the north component. Given the up-to-the-north propagation to this station, positive SV-polarity is thus indicated. There is, however, no clear signal on the east component (which, given the northward propagation, recorded primarily the SH-phase) until ~30 ms later, from which it can be inferred that the SH-wave arrival at this station may be 'nodal'.

If the first of these alternatives (i.e., negative SH-polarity and positive SV-polarity) for HHF is adopted for the time being, the focal mechanism is tightly constrained (Fig. S2); the orientation of its nodal planes (preferred strike 024°, dip 75°, and rake 170°) cannot be adjusted by more than a few degrees without contradicting one or other of the data. It can also be seen (Fig. S2(a)) that with this focal mechanism orientation the P-wave arrivals at PRH and AVH plot close to the null axis of the radiation pattern; their low amplitudes (which is what made picking difficult in the first place) can thus be explained. This solution is nonetheless consistent with the compressional P-wave arrivals picked by *Clarke et al*. [2014] at AVH and HHF, and could be made consistent with their dilatational pick at PRH by a very small adjustment. However, the measured maximum principal stress direction falls within a compressional quadrant of this focal mechanism or any other that can be formed by small adjustments consistent with these choices of polarity picks. This orientation can therefore be excluded.

I thus infer that the second of the alternative polarity choices for HHF (i.e., positive SH-polarity and negative SV-polarity) is correct. With this choice, the strike and dip of the focal mechanism happen to be quite tightly constrained at ~030° and ~75° but the rake is not; it can vary over a wide range up to circa -20° without violating any constraints from S-wave polarities. I therefore adopt a preferred solution with strike 030°, dip 75° and rake -20°, given the presumption that the largest component of differential stress is between the two horizontal principal stresses, thus a focal mechanism approximating strike-slip can be expected. This

revised focal mechanism is consistent with my compressional polarity pick at PRH and my picks of dilatations at AVH and HHF, although not with my pick of a dilatation at EVW. The relative strength of the compressional first motion at PRH and the weakness of the dilatation at HHF might be taken as indicating that the ESE-dipping nodal plane is steeper than I have drawn, and so plots farther from PRH and closer to HHF. However, any significant increase in dip of this nodal plane would require negative SV-polarity at PRH; I prefer to make the solution consistent with the S-wave evidence, this being clearer than the P-wave evidence. The ESE-dipping nodal plane of my focal mechanism is subparallel to the fault with strike 030° and dip 70° that has been imaged by seismic reflection profiling and is depicted in Fig. 4 of *Clarke et al*. [2014]. Notwithstanding the difficulties discussed in the main text regarding interpretation of seismic sections, I infer that this nodal plane was the fault plane. This event thus involved almost pure left-lateral strike slip, a slip sense compatible with the orientation of the stress tensor, given that the maximum principal stress lies in the dilatational quadrant.

The 27 May 2011 event (M_L 1.5), which yielded a three-component record at HHF and a vertical-component record at AVH, was investigated by *O'Toole et al*. [2013] using an experimental waveform-modeling technique. The location they determined (SD 37809 35606; easting ±28m; northing ±85m; depth 2343±2m) is close to mine for the 2 August event, consistent with my inferences that the induced seismicity occurred south of the Preese Hall-1 well and that the focal depth was within the depth range of the fracking and not significantly deeper. However, their confident statements of tight error margins, especially for focal depth, do not seem appropriate given the limited data available. Seismograms for this event were illustrated by *Eisner et al*. [2011], by *O'Toole et al*. [2013], and by *Clarke et al*. [2014; Fig. A5 in their online supplement 1]; the S-wave signals at HHF are, indeed, very similar those already discussed for the 2 August 2011 event. *O'Toole et al*. [2013] did not mark phase picks on those for HHF (although their waveform-modeling can match many observed features of the seismograms at this station), but it evident that they have regarded the initial low amplitude westward and southward pulses as the initial S-wave arrival, rather than the subsequent, stronger, eastward and northward pulses. By analogy with the aforementioned waveforms for the 2 August 2011 event, I favor this interpretation by *O'Toole et al*. [2013], rather than the *Eisner et al*. [2011] / *Clarke et al.* [2014] view that the first arrivals were the later strong eastward and northward pulses. However, although the focal mechanism that *O'Toole et al*. [2013] determined (strike 070°, dip 90°, rake 0°) correctly predicts the negative SV-polarity at station HHF, it would also predict negative SH-polarity at HHF, whereas the initial westward SH-pulse requires, given the southward propagation, positive polarity (Fig. S3). I do not understand why their best-fitting solution should incorporate this mismatch; however, the moment tensor, determined by *O'Toole et al*. [2013], that corresponds to this focal mechanism is subject to considerable uncertainty and can be rotated by as much as ~24° while keeping it within error bounds, an amount that is just about sufficient to move the position of HHF on the focal sphere into the positive quadrant of the SH-wave radiation pattern. Furthermore, although *Eisner et al*. [2011] reported the P-wave polarities as dilatational at AVH and compressional at HHF, *Clarke et al*. [2014] provided a clear illustration of the P-wave arrival at HHF, showing it to be a dilatational. The *O'Toole et al*. [2013] focal mechanism is inconsistent with the clear dilatational P-wave arrival at HHF, since this station plots on one of its nodal planes (Fig. S3). In my view the initial P-wave pulse at AVH is difficult to identify, suggesting a nodal first motion; this, together with my adoption of dilatational P-wave, negative SH-wave, and positive SV-wave polarities at HHF, are consistent with my preferred focal mechanism for the 2 August 2011 event, suggesting that both events had very similar focal mechanisms, as others [e.g., *de Pater and Baisch*, 2011; *Eisner et al*., 2011; *Clarke et al*., 2014] have previously argued on the basis of similarities in waveforms. If so, the interpretation of a nodal P-wave dilatation at AVH imposes a strong constraint of the rake of this focal mechanism, as any value significantly more negative than -20° would place this station in the compressional quadrant of its P-wave radiation pattern.

References

Aki, K., and P. G. Richards (1980). Quantitative Seismology. W.H. Freeman, San Francisco, 932 pp.

BGS (2015). Coordinate converter. Available online: http://www.bgs.ac.uk/data/webservices/convertForm.cfm (accessed 28 March 2015).

Clarke, H., L. Eisner, P. Styles, and P. Turner (2014). Felt seismicity associated with shale gas hydraulic fracturing: The first documented example in Europe. *Geophysical Research Letters*, *41*, 8308–8314.

de Pater, C. J., and S. Baisch (2011). Geomechanical study of Bowland Shale seismicity: synthesis report. Cuadrilla Resources Ltd., Lichfield, 71 pp. Available online: http://www.rijksoverheid.nl/bestanden/documenten-en-publicaties/rapporten/2011/11/04/rapport-geomechanical-study-of-bowland-shale-seismicity/rapport-geomechanical-study-of-bowland-shale-seismicity.pdf (accessed 5 April 2015)

Eisner, L., E. Janská, I. Opršal, and P. Matoušek (2011). Final Report: Seismic analysis of the events in the vicinity of the Preese Hall well. Seismik s.r.o., Prague, Czech Republic, 29 pp. Available online: http://www.cuadrillaresources.com/wp-content/uploads/2012/02/Geomechanical-Study-Appendix-3-2.11.2011.pdf (accessed 8 March 2015)

Fisher, K., and N. Warpinski (2012). Hydraulic-fracture-height growth: Real data. *Society of Petroleum Engineers, Productions and Operations Journal*, *27*, 8–19.

Galloway, D. D. (2012). Bulletin of British Earthquakes 2011. British Geological Survey Internal Report, OR/12/041. British Geological Survey, Edinburgh, 46 pp. Available online: http://www.earthquakes.bgs.ac.uk/publications/bulletins/Eqbull2011.pdf (accessed 8 March 2015)

Kirby, G. A., H. E. Baily, R. A. Chadwick, D. J. Evans, D. W. Holliday, S. Holloway, A. G. Hulbert, T. C. Pharaoh, N. J. P. Smith, N. Aitkenhead, and B. Birch (2000). The structure and evolution of the Craven Basin and adjacent areas. Subsurface memoir. The Stationery Office, London, 130 pp.

O'Toole, T., J. P. Verdon, J. H. Woodhouse, and J. M. Kendall (2013), Induced seismicity at Preese Hall, UK—A review. 75th EAGE Conference and Exhibition incorporating SPE EUROPEC 2013, London. Extended abstract, 5 pp, doi: 10.3997/2214-4609.20130011. Available online: http://www.earthdoc.org/publication/publicationdetails/?publication=68869 (accessed 27 March 2015)

Seismik (2012). Preliminary report to Cuadrilla Resources, 13/01/2012. Seismik s.r.o., Prague, Czech Republic, 45 pp. Available online: https://www.gov.uk/government/uploads/system/uploads/attachment_data/file/15742/5071-annex-g.pdf (accessed 8 March 2015)

Westaway, R., and P. L. Younger (2014). Quantification of potential macroseismic effects of the induced seismicity that might result from hydraulic fracturing for shale gas exploitation in the UK. *Quarterly Journal of Engineering Geology and Hydrogeology*, *47*, 333–350.

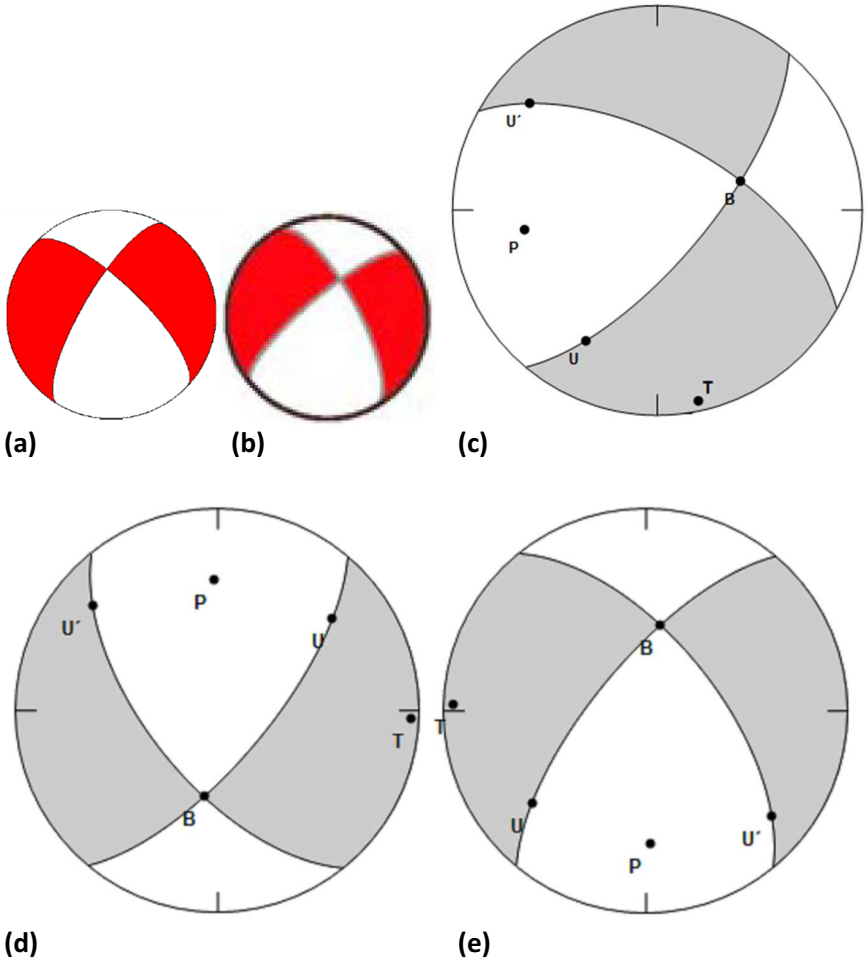

Figure S1. Depictions of the P-wave focal mechanism of the 2 August 2011 earthquake, with compressional quadrants shaded. See supplementary text S1 for discussion. (a) Focal mechanism reported as having strike 60°, dip 65°, and rake -150°, from *Seismik* [2012]; no type of projection was specified. (b) Focal mechanism reported as having strike 40°, dip 70°, and rake -150°, from *Clarke et al*. [2014]; reported as a lower focal hemisphere projection of unspecified geometry. The same data and same (unexplained) method seems to have been used as for the solution in (a), so the change in orientation must relate to the adoption of a different hypocentral location. (c) Correct lower focal hemisphere, equal area projection, for the focal mechanism orientation (strike 40°, dip 70°, rake -150°) specified for (b). (d) Lower focal hemisphere, equal area projection, for a focal mechanism with strike 40°, dip 70°, and rake -30°. (e) Upper focal hemisphere, equal area projection, for a focal mechanism with strike 40°, dip 70°, and rake -30°. This latter diagram resembles that in (b), suggesting that *Clarke et al*. [2014] may in fact have drawn an upper focal hemisphere projection even though they stated that it was the lower focal hemisphere. However, if so, they must have measured rake in a left-handed sense, rather than following the right-handed convention that is standard in earthquake seismology. Nonetheless, even so, the diagram in (e) still differs somewhat from that in (b), raising the possibility that this might not be the correct explanation.

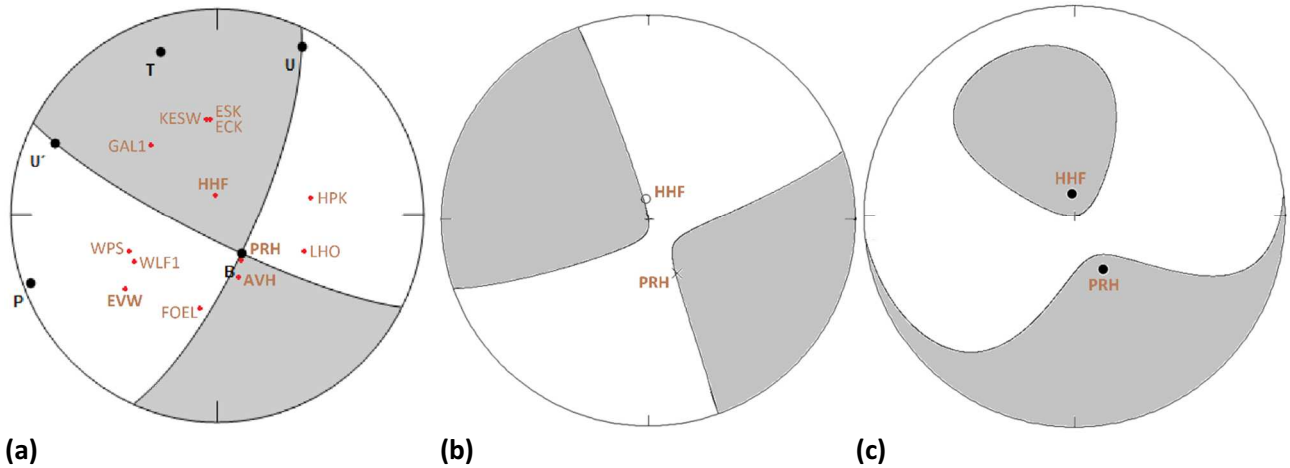

Figure S2. Potential focal mechanism (not preferred)for the 2 August 2011 earthquake (strike 24°, dip 75°, rake 170°, P-axis azimuth 250° with plunge 4°, and T-axis azimuth 341° with plunge 18°). All diagrams are equal area projections of the lower focal hemisphere, with compressional quadrants (for P-waves) and positive-polarity quadrants (for S-waves) shaded. Ray paths to local stations (annotated with bolder letters), which pass through the focal sphere upwards, have been projected in the opposite direction into the lower focal hemisphere. See supplementary text S1 for discussion. (a) P-wave radiation pattern showing local stations and positions on the focal sphere of the regional stations that recorded the 27 May 2011 event (the latter projected assuming the first motions are from Pg phases refracted horizontally along basement with V_p=6.45 km s^{-1}, from *Galloway* [2012], assuming V_p=4.00 km s^{-1} at the source; i.e., are assumed to plunge at 52°). Clear P-wave polarities are not apparent at these stations, according to *Galloway* [2012], but they are depicted so their potential impact on constraining the source orientation can be seen, in the event that future analysis (maybe involving very careful filtering of the seismograms – beyond the scope of the present study) might shed light on this aspect. (b) Corresponding SH-wave radiation pattern. (c) Corresponding SV-wave radiation pattern. Solid and open symbols in (b) and (c) denote signals of positive and negative polarity; cross in (b) denotes an unclear (? nodal) signal.

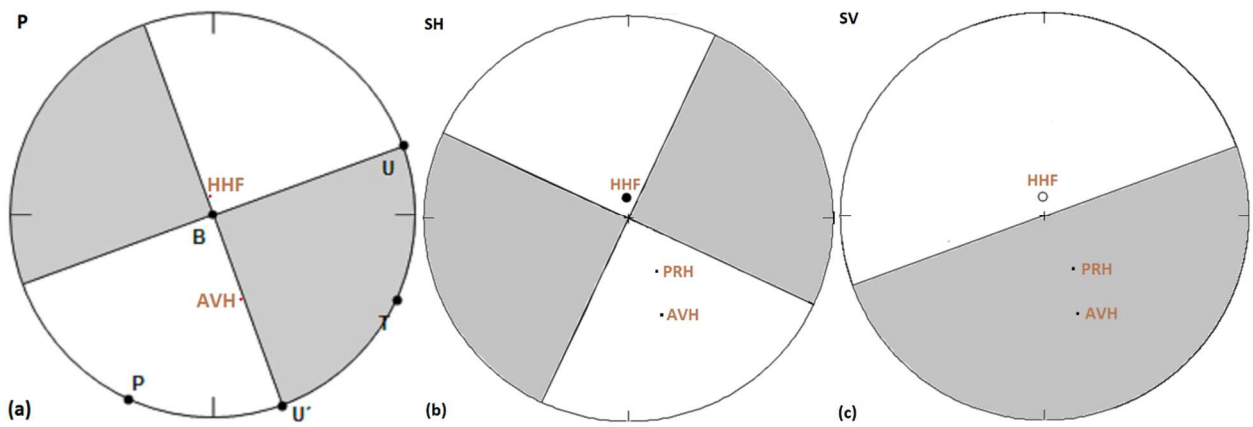

Figure S3. Preferred double couple focal mechanism for the 27 May 2011 earthquake (strike 070°, dip 90°, rake 0°) from *O'Toole et al*. [2013], using the same display format for local stations as Fig. S2. See supplementary text S1 for discussion. (a) P-wave radiation pattern. (b) Corresponding SH-wave radiation pattern. (c) Corresponding SV-wave radiation pattern.

Table S1: Temporary seismograph network

Code	BNG	Name
AVH	SD 3705 3781	Avenham Hall
HHF	SD 3775 3550	Hill House Farm
EVW	SD 4028 3797	East View
PRH	SD 3724 3674	Preese Hall

Co-ordinates, expressed as British National Grid (BNG) references, are listed to the nearest 10 m, based on map depictions by *Seismik* [2012] and in Fig. 1 of *Clarke et al*. [2014]. For comparison, the Preese Hall wellhead is at SD 37525 36584. BNG references such as these can be converted into geographical co-ordinates, if necessary, using standard software [e.g., *BGS*, 2015]. All seismographs were within the range ~10-20 m above sea-level, as is the Preese Hall-1 wellhead, so no corrections have been applied in the present analysis for differences in ground surface height.

Table S2. Seismic phases at temporary local stations

	P-waves										S-waves									
Code	t_{rp}	Δt_p	t_{op}	BNG_p	L_p (m)	D_p (m)	R_p (m)	α_p(°)	ϕ_{sp}(°)	ϕ_{op}(°)	t_{rs}	Δt_s	t_{os}	BNG_s	L_s (m)	D_s (m)	R_s (m)	α_s(°)	ϕ_{ss}(°)	ϕ_{os}(°)
HHF	9.991	0.626	9.365	SD 37720 35846	2524	347	2524	175.0	6.5	7.5	10.570	1.211	9.359	SD 37720 35844	2524	346	2524	175.0	6.1	8.4
PRH	9.991	0.667	9.324	SD 37714 35856	2697	1003	2694	331.8	17.8	20.7	10.661	1.298	9.363	SD 37730 35826	2712	1037	2707	331.8	17.2	23.9
AVH	10.060	0.799	9.261	SD 37718 35871	3248	2050	3233	341.0	31.0	36.6	-	1.568	-	SD 37737 35814	3297	2111	3272	341.0	29.3	42.2
EVW	-	1.043	-	SD 37635 35813	4280	3414	4231	50.8	39.9	48.0	-	1.980	-	SD 37727 35888	4204	3294	4136	50.8	36.0	53.8

For each seismic phase: t_r is the picked arrival time; Δt is the calculated travel time assuming the velocity model in Table S1 and a hypocentral depth of 2500 m; t_o is the estimated origin time (calculated as t_r - Δt); BNG is the British National Grid reference of the epicenter, calculated for this seismic phase recorded at this station; L is the length of the ray path; D is the epicentral distance; R is the hypocentral distance; α is the ray path azimuth; ϕ_s is the inclination, relative to the upward vertical, of the ray path at the Earth's surface; and ϕ_o is the inclination, relative to the upward vertical, of the ray path on leaving the hypocenter. Subscripts p and s denote P- and S-phases. Dashes for t_r and t_o indicate that no arrival time pick has been made.